Stability of parallel/perpendicular domain boundaries in lamellar block copolymers under oscillatory shear

Zhi-Feng Huang[a)] and Jorge Viñals

McGill Institute for Advanced Materials, and Department of Physics, McGill University, Montreal QC H3A 2T8, Canada

(Received 8 May 2006; final revision received 22 October 2006)

Synopsis

We introduce a model constitutive law for the dissipative stress tensor of lamellar phases to account for low frequency and long wavelength flows. Given the uniaxial symmetry of these phases, we argue that the dissipative stress tensor must be similar to that of nematics/smectics but with the local variable being the slowly varying lamellar wave vector. This assumption leads to a dependence of the effective dynamic viscosity on orientation of the lamellar phase. We then consider a model configuration comprising a domain boundary separating laterally unbounded domains of so called parallel and perpendicularly oriented lamellae in a uniform, oscillatory, shear flow, and show that the configuration can be hydrodynamically unstable for the constitutive law chosen. It is argued that this instability and the secondary flows it creates can be used to infer a possible mechanism for orientation selection in shear experiments. © *2007 The Society of Rheology.* [DOI: 10.1122/1.2399088]

I. INTRODUCTION

Recent interest in block copolymers arises from their ability to self-assemble at the nanoscale through microphase separation and ordering, leading to mesophases with various types of symmetries, such as lamellar, cylindrical, or spherical [Fredrickson and Bates (1996); Larson (1999)]. However, when processed by thermal quench or solvent casting from an isotropic, disordered state, a macroscopic sample manifests itself as a polycrystalline configuration consisting of locally ordered but randomly oriented domains (or grains), with the presence of large amount of topological defects and unusual rheological properties. The development of the equilibrium state characterized by macroscopic orientational order, as desired in most of applications, requires unrealistically long times; hence, external forces, such as steady or oscillatory shears are usually applied to accelerate domain coarsening and induce long range order. However, the mechanisms responsible for the response of the copolymer microstructure to the shear, and the selection of a particular orientation over a macroscopic scale are still poorly understood. In this paper we focus on the case of imposed oscillatory shear flows on lamellar phases of block copolymers and present an orientation selection mechanism originating from an effective viscosity contrast between lamellar phases of different orientation. Our study is

[a)]Author to whom correspondence should be addressed; Present address: Department of Physics and Astronomy, Wayne State University, Detroit, MI 48201; electronic mail: huang@physics.wayne.edu

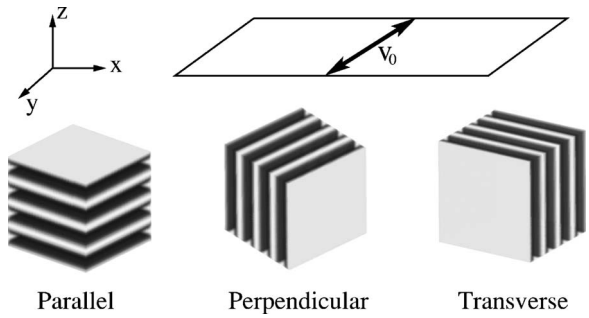

FIG. 1. Three lamellar orientations (Parallel, Perpendicular, and Transverse) under shear flow.

based on a mesoscopic or coarse grained description of a copolymer, but our results are expected to apply to other systems with the same symmetry as a microphase separated block copolymer.

Schematically, the response of lamellar block copolymers to external shear flow can be classified according to three possible uniaxial orientations (see Fig. 1): parallel (with lamellar planes parallel to the shearing surface), perpendicular (with lamellae normal along the vorticity direction of the shear flow), and transverse (with lamellae normal directed along the shear). Solid like or elastic response is expected for lamellar phases of transverse orientation, while fluid like or viscous response follows for the other two, leading to different rheological properties at low shear frequencies as measured experimentally [Koppi *et al.* (1992); Fredrickson and Bates (1996)]. It is known that both parallel and perpendicular alignments are favored over the transverse one under shear, and either of them would be ultimately selected by shear flow, as observed in most shear aligning experiments [Larson (1999)] (although some of the experimental work indicates a coexistence between parallel and transverse orientations [Pinheiro *et al.* (1996)], fact that might be a result of strong segregation and/or molecular entanglement). Of particular interest, and the least understood, is the selection between parallel and perpendicular orientations and its dependence on shear frequency ω and strain amplitude γ [Koppi *et al.* (1992); Maring and Wiesner (1997)] as well as temperature [Koppi *et al.* (1992); Pinheiro and Winey (1998)]. Near the order-disorder transition temperature T_{ODT} and at low shear frequencies, parallel alignment has been found in poly(ethylene-propylene)-poly-(ethylethylene) (PEP-PEE) samples [Koppi *et al.* (1992)], while for poly(styrene)-poly-(isoprene) (PS-PI) copolymers, the observed ultimate orientation is parallel [Maring and Wiesner (1997); Leist *et al.* (1999)] or perpendicular [Patel *et al.* (1995)], depending on sample processing details such as thermal history and shear starting time [Larson (1999)]. At higher but still intermediate frequencies (where $\omega < \omega_c$, with ω_c the characteristic frequency of polymer chain relaxation dynamics), the preferred orientation is perpendicular for both PEP-PEE and PS-PI copolymers under high enough shear strain [Koppi *et al.* (1992); Patel *et al.* (1995); Maring and Wiesner (1997); Leist *et al.* (1999)]. At high frequencies ($\omega > \omega_c$) the orientation selected is different for PEP-PEE (perpendicular) than PS-PI (parallel).

No basic understanding exists about the mechanisms underlying the above complex phenomenology of orientation selection despite intense theoretical scrutiny in recent years. For the frequency range $\omega < \omega_c$ that we are interested in here, the detailed relaxation dynamics of the polymer chains within each block are not expected to be important; thus one adopts a coarse grained, reduced description in terms of the local monomer

density as the order parameter [Leibler (1980); Ohta and Kawasaki (1986); Fredrickson and Helfand (1987)]. Most of the early analyses of shear alignment of copolymers relied on thermal fluctuation effects near the *transition point* T_{ODT}, and focused on the role of *steady shears*. A study by Cates and Milner (1989) indicates that in the vicinity of the order-disorder transition, steady shear would suppress critical fluctuations in an anisotropic manner, increase the transition temperature, and favor the perpendicular orientation. Further extension by Fredrickson (1994) by incorporating viscosity contrast between the microphases has shown that the perpendicular alignment becomes prevalent for high shear rates, while the parallel one would be favored at low shear rates.

Consideration was given later to situations that are not fluctuation dominated (such as well aligned lamellar phases or defect structures), regarding both stability and defect dynamics. Stability differences between uniform parallel and perpendicular structures subjected to *steady shears* have been found [Goulian and Milner (1995)] through the consideration of anisotropic viscosities in a uniaxial fluid. Recent molecular dynamics studies as well as hydrodynamic analyses of the smectic A phase [Soddemann *et al.* (2004); Guo (2006)] have shown an undulation instability of parallel lamellae, as well as a transition from fully ordered parallel to perpendicular phases for large enough shear rate. Regarding the effect of *oscillatory shears*, an analysis of secondary instabilities [Drolet *et al.* (1999); Chen and Viñals (2002)] has shown that the extent of the stability region for the perpendicular orientation is always larger than that of the parallel direction, and as expected, both much larger than the transverse region. Importantly, the role of viscosity difference between the polymer blocks [as introduced by Fredrickson (1994) to address shear effects near the transition point] is found to be negligible for the stability of well aligned lamellar structures, due to its weak coupling to long wavelength perturbations. In order to address experimental phenomenology described above related to domain coarsening and orientation selection, more recent theoretical efforts have focused on the dynamic competition between coexisting phases of different orientations. A recent example includes the study of a grain boundary separating parallel and transverse lamellar domains under oscillatory shears, and the dependence of the grain boundary velocity on shear parameters such as frequency and amplitude [Huang *et al.* (2003); Huang and Viñals (2004)].

However, we are still far from accounting for the existing experimental phenomenology on orientation selection, possibly because current approaches and models for block copolymer viscoelasticity might not be adequate. It is important to note that block copolymer viscous response is not Newtonian even in the limit of vanishing frequency $\omega \to 0$, since the Newtonian response would result in the degeneracy of parallel and perpendicular orientations, contrary to experimental findings. In the theory of Fredrickson (1994), the Newtonian assumption is used for individual microphases, with different Newtonian viscosities chosen for different monomers (blocks). We adopt here an alternative approach appropriate for flows on a scale much larger than the lamellar spacing and address the resulting deviation from Newtonian response in the low frequency limit. We introduce a constitutive law for the viscous stress tensor that explicitly incorporates the uniaxial character of lamellar phases in analogy with similar treatments of anisotropic fluids [Ericksen (1960); Leslie (1966)] and nematic and smectic liquid crystals [Forster *et al.* (1971); Martin *et al.* (1972); de Gennes and Prost (1993)]. As will be shown below, the resulting effective viscosity depends on lamellar orientation, in qualitative agreement with experimental results. Our analysis, however, only applies at low frequencies, well below the inverse relaxation time of the polymer chains. In this limit, chain entanglement effects that lead to elastic distortion at finite frequencies in parallel or perpendicular configurations [Williams and MacKintosh (1994)], would be absent. Therefore we only

focus on the viscous mechanism which, on account of the symmetry of lamellar phases, dominates the competition between parallel and perpendicular orientations at the lowest frequencies. Further discussion of this issue will be presented at the end of this paper.

The ultimate focus of our analysis is the competition among coexisting but differently oriented lamellar domains under oscillatory shears in a polycrystalline sample. Although we are primarily concerned here with a simplified configuration involving only two regions of parallel and perpendicular orientations, we use our results to infer a possible selection mechanism in multidomain configurations. We show below that an instability of hydrodynamic origin occurs at the interface separating parallel and perpendicular lamellae for certain ranges of material and shear parameters. The instability leads to nonuniform secondary flows which are argued to favor the perpendicular orientation in some ranges of parameters. A comparison of our results to existing experimental findings, as well as possible tests of our predictions, are also discussed.

II. MODEL

A. Governing equations

In the range of low shear frequencies compared to the inverse of the polymer chain relaxation time, the mesoscopic description of a block copolymer is based on an order parameter field ψ representing the variation of local monomer density, and a velocity field $\mathbf{v}$. The evolution of ψ is governed by a time dependent Ginzburg–Landau equation

$$\partial\psi/\partial t + \mathbf{v}\cdot\boldsymbol{\nabla}\psi = -\Lambda\,\delta\mathcal{F}/\delta\psi, \tag{1}$$

with $\mathcal{F}$ as the coarse grained free energy given by Leibler (1980) and Ohta and Kawasaki (1986), and Λ as an Onsager kinetic coefficient. Equation (1) is coupled to the following equation governing the local velocity field $\mathbf{v}=(v_x,v_y,v_z)$:

$$\mathrm{Re}(\partial\mathbf{v}/\partial t + \mathbf{v}\cdot\boldsymbol{\nabla}\mathbf{v}) = -\boldsymbol{\nabla}p + \boldsymbol{\nabla}\cdot\boldsymbol{\sigma}^D, \tag{2}$$

with the incompressibility condition $\boldsymbol{\nabla}\cdot\mathbf{v}=0$. Here p is the pressure field, and Re is the Reynolds number defined as

$$\mathrm{Re} = \rho\omega d^2/\eta \tag{3}$$

with ω as the shear flow frequency, d as the thickness of copolymer system confined between two shear planes, ρ as the copolymer density, and η as a Newtonian viscosity. The coupling in Eqs. (1) and (2) is complex, especially when the stress tensor $\boldsymbol{\sigma}^D$ in Eq. (2) depends on the concentration field ψ, and when fluid inertia cannot be ignored (i.e., at nonzero Reynolds number). In order to simplify our analysis, we will first assume that order parameter diffusion in Eq. (1) is negligible, so that ψ is advected by the flow $\mathbf{v}$. At the end of the analysis, we will discuss possible implications of the flow fields obtained on order parameter diffusion as given by Eq. (1).

Equation (2) has been made dimensionless by introducing a length scale d, a time scale ω^{-1}, and by rescaling pressure $p\to p/(\eta\omega)$. It includes a dissipative stress tensor $\boldsymbol{\sigma}^D$ appropriate for a phase with uniaxial symmetry. We assume the constitutive equation (in dimensionless form) due to Ericksen [Ericksen (1960); Leslie (1966)] as originally derived for anisotropic fluids

$$\sigma^D_{ij} = D_{ij} + \alpha_1\hat{n}_i\hat{n}_j\hat{n}_k\hat{n}_l D_{kl} + \alpha_{56}(\hat{n}_i\hat{n}_k D_{jk} + \hat{n}_j\hat{n}_k D_{ik}), \tag{4}$$

where $D_{ij}=\partial_i v_j+\partial_j v_i$ $(i,j=x,y,z)$, but with $\hat{\mathbf{n}}=(\hat{n}_x,\hat{n}_y,\hat{n}_z)$ a unit vector defining the *slowly varying* local normal of the lamellar phase. Equation (4) is expected to be generic for any

uniaxial phase, and thus should apply to the lamellar phases studied here by reason of symmetry. There are two independent viscosities α_1 and α_{56} [the Leslie's coefficients in the notation used by de Gennes and Prost (1993)], which have been rescaled as

$$\alpha_1 \to \alpha_1/\eta \quad \text{and} \quad \alpha_{56} \to \alpha_{56}/\eta.$$

They obey the relationship (due to the positivity of entropy production [Forster *et al.* (1971); Martin *et al.* (1972)])

$$\alpha_{56} \geqslant -1 \quad \text{and} \quad \alpha_1 + 2\alpha_{56} \geqslant -1. \tag{5}$$

Equation (4) is justified on symmetry grounds, and we note that a similar constitutive relation also appears in the viscous stress of other uniaxial phases such as nematic or smectic liquid crystals [Forster *et al.* (1971); Martin *et al.* (1972); de Gennes and Prost (1993); Larson (1999)]. However, the viscous stress we assume here for a lamellar block copolymer does not include all the Leslie viscosities in the Leslie–Ericksen equation used for nematics which, as compared to Eq. (4), has two extra terms related to the director rotation rate of the molecules. As in smectics A, the independent degree of freedom provided by this rotation of the molecular director is absent in a lamellar phase, for which the director field has been replaced by the local lamellar normal as indicated in Eq. (4).

Given a range of possible different viscous stresses, as well as different elastic responses, function of the order parameter appropriate for each system {the Leibler [Leibler (1980)] or Ohta–Kawasaki [Ohta and Kawasaki (1986)] energy for block copolymers, the Frank–Oseen distortion energy for nematics, and the compression bending energy for smectics A [de Gennes and Prost (1993); Larson (1999)]}, one can anticipate that the general rheological response will vary with the type of uniaxial system under consideration (lamellar block copolymers, nematic and smectic liquid crystals), even though the constitutive relation (4) should apply to all of them. However, in the low frequency limit in which the details of the molecular relaxation play only a secondary role, a well aligned lamellar block copolymer is expected to belong to the same class as smectics A due to the analogy of mechanical properties [Amundson and Helfand (1993)] and of rheological behavior [Larson *et al.* (1993)], though both of them differ from nematics. Hence, the configuration studied below (as introduced in Sec. II B) can also be understood as that of two stacked smectics. Note, however, that in the case of a block copolymer the existence and stability of such a configuration in the absence of flow follows from the stability of microphase separated phases.

In addition to the anisotropic, zero frequency, viscous dissipation just described, we note that there exists an additional contribution to dissipation arising from order parameter diffusion, as given by the relaxation of the order parameter field ψ given in Eq. (1) [Ohta *et al.* (1993)]. However, this contribution, although nonzero in the small frequency limit in which we assume the constitutive law (4), is neglected in the analysis below as we do not explicitly consider order parameter relaxation.

For a uniform lamellar phase of parallel orientation [$\hat{\mathbf{n}} = (0,0,1)$ for the imposed shear flow along the y direction considered, see Fig. 1], the equations governing the velocity field can be written explicitly as

$$\begin{aligned}
\mathrm{Re}(\partial_t v_x + v_j \partial_j v_x) &= -\partial_x p + \partial_j^2 v_x + \alpha_{56}(\partial_z^2 v_x + \partial_x \partial_z v_z), \\
\mathrm{Re}(\partial_t v_y + v_j \partial_j v_y) &= -\partial_y p + \partial_j^2 v_y + \alpha_{56}(\partial_z^2 v_y + \partial_y \partial_z v_z),
\end{aligned} \tag{6}$$

$$\mathrm{Re}(\partial_t v_z + v_j \partial_j v_z) = -\partial_z p + (1+\alpha_{56})\partial_j^2 v_z + 2(\alpha_1+\alpha_{56})\partial_z^2 v_z,$$

after substitution of Eq. (4) into Eq. (2). For a domain of perpendicular orientation [$\hat{\mathbf{n}}=(1,0,0)$] we have instead

$$\mathrm{Re}(\partial_t v_x + v_j \partial_j v_x) = -\partial_x p + (1+\alpha_{56})\partial_j^2 v_x + 2(\alpha_1+\alpha_{56})\partial_x^2 v_x,$$

$$\mathrm{Re}(\partial_t v_y + v_j \partial_j v_y) = -\partial_y p + \partial_j^2 v_y + \alpha_{56}(\partial_x^2 v_y + \partial_x \partial_y v_x), \tag{7}$$

$$\mathrm{Re}(\partial_t v_z + v_j \partial_j v_z) = -\partial_z p + \partial_j^2 v_z + \alpha_{56}(\partial_x^2 v_z + \partial_x \partial_z v_x).$$

The Newtonian limit is recovered by setting $\alpha_1=\alpha_{56}=0$. Contrary to previous work on block copolymers in the creeping flow approximation [Goulian and Milner (1995); Fredrickson (1994); Chen and Viñals (2002)], we retain inertial terms in the above equations. Although small, they are significant in determining the instabilities discussed below. In the regime of small Re, both uniform parallel and perpendicular configurations are hydrodynamically stable as derived from Eqs. (6) and (7) with a procedure similar to that shown in Sec. III for the grain boundary configuration.

Our assumption, Eq. (4), is consistent with experimental determinations of the loss modulus G'' and dynamic viscosity η' ($=G''/\omega$) for uniform phases of different lamellar orientations. Assuming a shear flow along y (Fig. 1), we have in the creeping flow limit $\mathrm{Re}\to 0$ (in dimensional form)

- Perpendicular [$\hat{\mathbf{n}}=(1,0,0)$]: $\eta'=\eta$;
- Parallel [$\hat{\mathbf{n}}=(0,0,1)$]: $\eta'=\eta+\alpha_{56}$;
- Transverse [$\hat{\mathbf{n}}=(0,1,0)$]: $\eta'=\eta+\alpha_{56}+[2a^2/(1+a^2)^2]\alpha_1$ [$a=\gamma\sin(\omega t)$, with γ the shear strain amplitude]; when averaged over period T, it is $\langle\eta'\rangle_T=\eta+\alpha_{56}+[\gamma^2/(1+\gamma^2)^{3/2}]\alpha_1$.

When $\alpha_1>0$ and $\alpha_{56}>0$, we obtain $\eta'_{\mathrm{Transverse}}>\eta'_{\mathrm{Parallel}}>\eta'_{\mathrm{Perpendicular}}$, in agreement with low ω experimental results of Koppi *et al.* (1992) for PEP-PEE diblock copolymers, and also with the result of molecular dynamics simulations by Guo (2006) showing smaller viscosity of perpendicular lamellae compared to that of the parallel phase. On the other hand, when $\alpha_{56}<0$, we have $\eta'_{\mathrm{Parallel}}<\eta'_{\mathrm{Perpendicular}}$, which is the case in PS-PI copolymers [Chen and Kornfield (1998); Gupta *et al.* (1995)]. The viscosity coefficients α_1 and α_{56} could be in principle measured in block copolymers under shear flows, with experimental setups possibly similar to those used in nematic liquid crystals [see, e.g., methods reviewed by de Gennes and Prost (1993)].

B. Parallel/perpendicular configuration and viscosity contrast

We focus on coexisting lamellar domains of parallel and perpendicular orientations under oscillatory shear flows. In real samples these two types of domains may be separated by topological defects such as grain boundaries, dislocations, or disclinations. We study here the simplified configuration shown in Fig. 2, comprising two fully ordered, three dimensional lamellar domains that are identical except for their orientation and thickness. The perpendicular domain A is of thickness d_A, and the parallel domain B of $d_B=1-d_A$ (in dimensionless form), both confined between a pair of shearing planes. The system is uniformly sheared along the y direction; the velocity field $\mathbf{v}$ is zero on the lower boundary plane $z=0$ and equal to $\mathbf{v}_0=\gamma\cos t\hat{\mathbf{y}}$ [or $\gamma\omega d\cos(\omega t)\hat{\mathbf{y}}$ in dimensional form] on the upper boundary $z=1$.

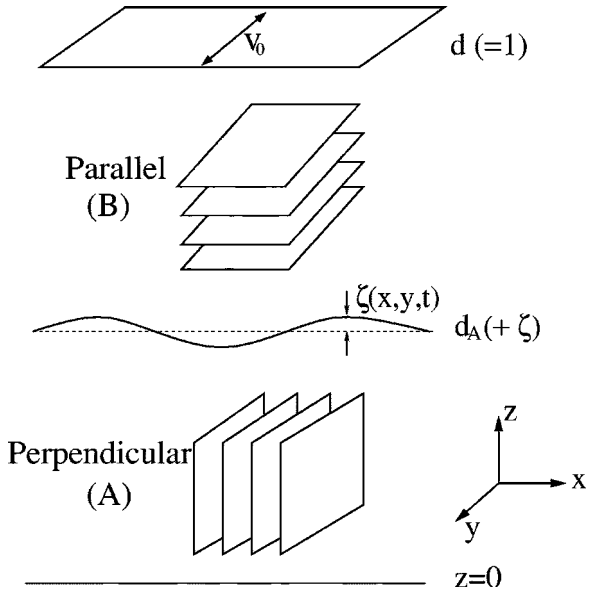

FIG. 2. A parallel/perpendicular configuration subjected to oscillatory shear flow.

Note that in the absence of external shear, a configuration analogous to that in Fig. 2 can exist in lamellar block copolymer samples, but not in liquid crystals with the same uniaxial symmetry, as found in various experiments [Gido *et al.* (1993); de Gennes and Prost (1993)]. Grain boundaries separating differently oriented domains have been observed in block copolymers, but are usually unstable (for large angles) in smectic A liquid crystals. The difference between the two cases can be explained by the difference in their respective order parameters, the free energy governing distortions, and the relaxation of the different types of individual molecules. Here we are interested in block copolymer systems in which the two domain configuration of Fig. 2 is known to be a stationary solution of the mesoscopic model, fact that results from the microphase separation.

Under the shear considered here, bulk configurations of either orientation (parallel or perpendicular) are linearly stable. However, we will show that the configuration of Fig. 2 can become unstable. Note that the effective viscosities of the two domains are different, as discussed in Sec. II A. Therefore this configuration is analogous to the case of two superposed Newtonian fluids of different viscosity, which is known to be unstable under steady {plane Couette flow [Yih (1967); Hooper (1985)]} or oscillatory [King *et al.* (1999)] shears. In the present case, however, the viscosity contrast follows from the orientation dependence of our constitutive law (4). This contrast between the lamellar phases can cause interface instability, but with a dependence on shearing conditions and system parameters much more complicated than that of the Newtonian limit.

III. HYDRODYNAMIC STABILITY ANALYSIS

A. Base flow

The base state for the configuration of Fig. 2 is a planar interface located at $z=d_A$, separating two stable perpendicular (A) and parallel (B) regions. Under uniform shear the velocity fields are along the y direction: $\mathbf{v}_{A,B}=(0,V_{A,B},0)$. In dimensionless form, the velocities are given by

$$V_A = \mathrm{Real}\{\alpha_A \sinh[(1+i)\beta_A z]\gamma e^{it}\},$$
$$V_B = \mathrm{Real}\{\alpha_A (\sinh[(1+i)\beta_A d_A]\cosh[(1+i)\beta_B(z-d_A)] + \sqrt{m}\cosh[(1+i)\beta_A d_A]\sinh[(1+i)\beta_B(z-d_A)])\gamma e^{it}\}, \tag{8}$$

with

$$\alpha_A^{-1} = \sinh[(1+i)\beta_A d_A]\cosh[(1+i)\beta_B d_B] + \sqrt{m}\cosh[(1+i)\beta_A d_A]\sinh[(1+i)\beta_B d_B]$$

and the viscosity ratio $m=\mu_A/\mu_B$ (with $\mu_A=1$ for the perpendicular region and $\mu_B=1+\alpha_{56}$ for a parallel domain). Here β_A and β_B are the inverse Stokes layer thicknesses

$$\beta_{A,B} = \left(\frac{\mathrm{Re}}{2\mu_{A,B}}\right)^{1/2}. \tag{9}$$

Also for the pressure field, $p_A=p_B=p_0$. Note that these base state solutions are the same as those of two superposed Newtonian fluids with different viscosities μ_A and μ_B under oscillatory Couette flow [King *et al.* (1999)].

B. Perturbation analysis

For Newtonian fluids or in some viscoelastic models (e.g., Oldroyd B or Maxwell fluids), the three dimensional stability problem can be reduced to an effective two dimensional one, with fluid stability under shear flows governed by Orr–Sommerfeld type equations for a single stream function describing two dimensional disturbances. However, this is not the case discussed here and governed by Eqs. (2) and (4), as will be seen below.

We expand both velocity and pressure fields into the base state given above and perturbations,

$$v_i^{A,B} = V_{A,B}\delta_{iy} + u_i^{A,B}\ (i=x,y,z), \quad p_{A,B} = p_0 + p'_{A,B}. \tag{10}$$

These flow perturbations are accompanied by an undulation of interface, denoted as $\zeta(x,y,t)$ (see Fig. 2). The boundary conditions at $z=d_A+\zeta(x,y,t)$ include:

continuity of velocity

$$\mathbf{v}^A = \mathbf{v}^B, \tag{11}$$

continuity of tangential stress

$$\{[1-(\partial_x\zeta)^2]\sigma_{xz}^D - \partial_x\zeta\partial_y\zeta\sigma_{yz}^D - \partial_y\zeta\sigma_{xy}^D + (\sigma_{zz}^D - \sigma_{xx}^D)\partial_x\zeta\}_A^B = 0, \tag{12}$$

$$\{[1-(\partial_y\zeta)^2]\sigma_{yz}^D - \partial_x\zeta\partial_y\zeta\sigma_{xz}^D - \partial_x\zeta\sigma_{xy}^D + (\sigma_{zz}^D - \sigma_{yy}^D)\partial_y\zeta\}_A^B = 0, \tag{13}$$

and balance of normal stress

$$\{-p + \sigma_{zz}^D - \partial_x\zeta\sigma_{xz}^D - \partial_y\zeta\sigma_{yz}^D\}_A^B = -\Gamma'(\partial_x^2\zeta + \partial_y^2\zeta), \tag{14}$$

where $\{\ \}_A^B = \{\ \}_B - \{\ \}_A$, σ_{ij}^D is the dissipative stress tensor, and

$$\Gamma' = \Gamma/(\eta\omega d), \tag{15}$$

with Γ the interfacial tension. Also, the kinematic condition at the interface yields

$$(\partial_t + \mathbf{v}^B\cdot\boldsymbol{\nabla})\zeta = v_z^B. \tag{16}$$

Assume expansions of the form

$$u_i^{A,B} = \sum_{q_x,q_y} \hat{u}_i^{A,B}(q_x,q_y,z,t)\exp[i(q_x x + q_y y)], \tag{17}$$

where q_x and q_y are wave numbers in the x and y directions. Substituting Eq. (17) into Eqs. (6) and (7), retaining terms up to first order in the perturbation amplitudes, and eliminating the pressure, we obtain the equations for the perturbed velocity fields $\hat{u}_z^{A,B}$ and $\hat{u}_x^{A,B}$, which govern the system stability when combined with the interfacial boundary conditions.

For the parallel region B ($d_A \leqslant z \leqslant 1$) we find

$$\mathrm{Re}[(\partial_t + iq_y V_B)(\partial_z^2 - q^2)\hat{u}_z^B - iq_y(\partial_z^2 V_B)\hat{u}_z^B] = (1+\alpha_{56})(\partial_z^2 - q^2)^2\hat{u}_z^B - 2\alpha_1 q^2\partial_z^2\hat{u}_z^B, \tag{18}$$

$$\begin{aligned}&\mathrm{Re}[\partial_t(\partial_z^2 - q^2)\hat{u}_x^B + iq_y(\partial_z^2 - q^2)(V_B\hat{u}_x^B) + 2q_x q_y(\partial_z V_B)\hat{u}_z^B]\\ &\quad = (\partial_z^2 - q^2)^2\hat{u}_x^B + \alpha_{56}(\partial_z^2 - q^2)(\partial_z^2\hat{u}_x^B - iq_x\partial_z\hat{u}_z^B) - 2iq_x\alpha_1\partial_z^3\hat{u}_z^B,\end{aligned} \tag{19}$$

(here $q^2 = q_x^2 + q_y^2$), while for the perpendicular region A ($0 \leqslant z \leqslant d_A$) we obtain

$$\begin{aligned}&\mathrm{Re}[(\partial_t + iq_y V_A)(\partial_z^2 - q^2)\hat{u}_z^A - iq_y(\partial_z^2 V_A)\hat{u}_z^A]\\ &\quad = (\partial_z^2 - q^2)^2\hat{u}_z^A - \alpha_{56}q_x^2(\partial_z^2 - q^2)\hat{u}_z^A + iq_x[2\alpha_1 q_x^2 - \alpha_{56}(\partial_z^2 - q^2)]\partial_z\hat{u}_x^A,\end{aligned} \tag{20}$$

$$\begin{aligned}&\mathrm{Re}[\partial_t(\partial_z^2 - q^2)\hat{u}_x^A + iq_y(\partial_z^2 - q^2)(V_A\hat{u}_x^A) + 2q_x q_y(\partial_z V_A)\hat{u}_z^A]\\ &\quad = (1+\alpha_{56})(\partial_z^2 - q^2)^2\hat{u}_x^A - 2\alpha_1 q_x^2(\partial_z^2 - q_y^2)\hat{u}_x^A,\end{aligned} \tag{21}$$

with rigid boundary conditions on the planes $z=0$ and $z=1$,

$$\begin{aligned}&\hat{u}_x^A(0) = \hat{u}_z^A(0) = \partial_z\hat{u}_x^A(0) = \partial_z\hat{u}_z^A(0) = 0,\\ &\hat{u}_x^B(1) = \hat{u}_z^B(1) = \partial_z\hat{u}_x^B(1) = \partial_z\hat{u}_z^B(1) = 0.\end{aligned} \tag{22}$$

The other velocity component $\hat{u}_y^{A,B}$ can be obtained from the incompressibility condition. Note that the form of Eqs. (18)–(21) is similar to that of the Orr–Sommerfeld equation for Newtonian fluids; however, in the above equations velocity fields are coupled (except for $q_x=0$), and thus the three dimensional system here cannot be reduced to an effective two dimensional one described by only one stream function. This irreducibility might be understood from the fact that parallel and perpendicular orientations can be distinguished only in three dimensional space, and thus the results of the associated flows that are orientation dependent should be also three dimensional.

The solutions to the above problem can be found by writing

$$\begin{aligned}\hat{u}_z^{A,B}(z,t) &= e^{\sigma t}\phi_z^{A,B}(z,t),\\ \hat{u}_x^{A,B}(z,t) &= e^{\sigma t}\phi_x^{A,B}(z,t),\\ \hat{\zeta}(t) &= e^{\sigma t}h(t),\end{aligned} \tag{23}$$

with interfacial perturbation $\hat{\zeta}$ defined by $\zeta(x,y,t) = \Sigma_{q_x,q_y}\hat{\zeta}(t)\exp[i(q_x x + q_y y)]$. When $q_y \neq 0$, according to Floquet's theorem $\phi_{z,x}^{A,B}$ and h are periodic in time t with period T ($=2\pi$ here) if the eigenvalue σ (the Floquet exponent) is simple [Yih (1968)], since coefficients in Eqs. (18)–(21) that are proportional to the base flow $V_{A,B}$ are periodic in t as shown in Eq. (8). When $q_y=0$, $\phi_{z,x}^{A,B}$ and h are time independent, and σ represents the perturbation growth rate. In either case, the real part of σ determines the system stability.

C. Small Reynolds number limit

The Newtonian viscosity η is very large for block copolymers, resulting in small Reynolds numbers [Eq. (3)]. For a typical block copolymer of density $\rho \sim 1$ g cm^{-3} and $\eta \sim 10^4 - 10^6$ P, Re/$\omega \sim 10^{-4} - 10^{-6}$ s for a thickness $d \sim 1$ cm. Within a reasonable range of frequencies ω of interest, we have Re $\ll 1$. The stability problem can be now solved analytically by expanding around small Reynolds number

$$\phi^{A,B}_{z,x}(z,t) = \phi^{A,B}_{(z,x)0}(z,t) + \mathrm{Re}\ \phi^{A,B}_{(z,x)1}(z,t) + \cdots,$$

$$h = h_0(t) + \mathrm{Re}\ h_1(t) + \cdots, \tag{24}$$

$$\sigma = \sigma_0 + \mathrm{Re}\ \sigma_1 + \cdots,$$

with ϕ and h functions defined in Eq. (23). Note that the order of the rescaled interfacial tension Γ', defined in Eq. (15) is ω dependent, and needs to be addressed separately. In the limit of Re $\to 0$ with Γ' finite, we set $\Gamma' = \Gamma_0 = \mathcal{O}(1)$, while for small but finite values of Reynolds numbers, Γ' can be expressed as a power of Re. For a typical value of $\Gamma \sim 1$ dyn/cm {the order of Γ can be estimated from the grain boundary interfacial energy calculated by self consistent field theory [Matsen (1997); Netz *et al.* (1997)]} and large η ($\sim 10^4 - 10^6$ P) appropriate for block copolymers, we have $\Gamma'\omega \sim 10^{-4} - 10^{-6}$ s^{-1}. The intermediate range of ω (around 1 s^{-1}) for typical experiments leads to $\Gamma' \equiv \mathrm{Re}\,\Gamma_1 = \mathcal{O}(\mathrm{Re})$, whereas for much larger frequencies $\Gamma'/\mathrm{Re} \ll 1$. In the following, we present the solutions of zeroth order (containing Γ_0) and first order (containing Γ_1) in Re, which are accurate enough to determine the stability behavior for lamellar block copolymers with typical Re $\ll 1$.

1. Re $\to 0$ *[with* $\Gamma' = \Gamma_0 = \mathcal{O}(1)$*]*

In this parameter range, we only need the zeroth order solution for the velocity fields, given by (for $q_x \neq 0$),

$$\phi^B_{z0} = B^{(0)}_1 e^{b_1 z} + B^{(0)}_2 e^{b_2 z} + B^{(0)}_3 e^{b_3 z} + B^{(0)}_4 e^{b_4 z}, \tag{25}$$

$$\phi^B_{x0} = C^{(0)}_1 e^{r_1 z} + C^{(0)}_2 e^{r_2 z} + C^{(0)}_3 e^{r_3 z} + C^{(0)}_4 e^{r_4 z} + \frac{iq_x}{q^2}\partial_z \phi^B_{z0}, \tag{26}$$

$$\phi^A_{z0} = A^{(0)}_1 e^{a_1 z} + A^{(0)}_2 e^{a_2 z} + A^{(0)}_3 e^{a_3 z} + A^{(0)}_4 e^{a_4 z} + D^{(0)}_1 A'_1 e^{s_1 z} + D^{(0)}_2 A'_2 e^{s_2 z} + D^{(0)}_3 A'_3 e^{s_3 z} + D^{(0)}_4 A'_4 e^{s_4 z}, \tag{27}$$

$$\phi^A_{x0} = D^{(0)}_1 e^{s_1 z} + D^{(0)}_2 e^{s_2 z} + D^{(0)}_3 e^{s_3 z} + D^{(0)}_4 e^{s_4 z}, \tag{28}$$

with

$$b_i^2 = \frac{q^2}{\mu_B}\{\mu_B + \alpha_1 \pm [\alpha_1(2\mu_B + \alpha_1)]^{1/2}\}, \tag{29}$$

$$s_i^2 = \{\mu_B q^2 + \alpha_1 q_x^2 \pm q_x^2[\alpha_1(2\mu_B + \alpha_1)]^{1/2}\}/\mu_B, \tag{30}$$

$$A'_i = iq_x\left(\frac{2\alpha_1 - \alpha_{56}^2}{s_i^2 - q^2 - \alpha_{56} q_x^2} - \frac{\mu_B}{q_x^2}\right)s_i \tag{31}$$

for $i = 1, 2, 3, 4$, and

$$r_1 = q, \quad r_2 = -q, \quad r_3 = q/\sqrt{\mu_B}, \quad r_4 = -q/\sqrt{\mu_B}, \tag{32}$$

$$a_1 = q, \quad a_2 = -q, \quad a_3 = \sqrt{q^2 + \alpha_{56} q_x^2}, \quad a_4 = -a_3. \tag{33}$$

For $q_x = 0$, we have $\phi^A_{x0} = \phi^B_{x0} = 0$, ϕ^B_{z0} is also given by Eq. (25), and

$$\phi^A_{z0} = (A_1^{(0)} + A_2^{(0)} z) e^{qz} + (-A_1^{(0)} + A_3^{(0)} z) e^{-qz}. \tag{34}$$

By using the boundary conditions (22), we can express the coefficients $A^{(0)}_{3,4}$, $B^{(0)}_{3,4}$, $C^{(0)}_{3,4}$, and $D^{(0)}_{3,4}$ in terms of $A^{(0)}_{1,2}$, $B^{(0)}_{1,2}$, $C^{(0)}_{1,2}$, and $D^{(0)}_{1,2}$. The remaining coefficients are obtained by solving a linear matrix equation

$$\boldsymbol{\chi} \cdot \boldsymbol{A}^{(0)} = \boldsymbol{h}^{(0)} h_0, \tag{35}$$

where $\boldsymbol{A}^{(0)} = [A_j^{(0)}, B_j^{(0)}, C_j^{(0)}, D_j^{(0)}]$ $(j = 1, 2)$ for $q_x \neq 0$ or $[A_j^{(0)}, B_j^{(0)}]$ for $q_x = 0$, $\boldsymbol{\chi}$ is an 8×8 or 4×4 constant matrix determined by the interfacial conditions (11)–(14), $h_0 = h_0(t)$ denotes the zeroth order interface perturbation, and the matrix $\boldsymbol{h}^{(0)}$ is a function of Γ_0 and $(\partial_z V_B)_0$, with $(\partial_z V_B)_0$ the gradient of zeroth order base flow $V_B^{(0)}$:

$$V_B^{(0)} = [\lambda_0 d_A + \delta(z - d_A)] \gamma \cos t, \quad (\partial_z V_B)_0 = \delta \gamma \cos t, \tag{36}$$

with

$$\delta = m\lambda_0, \quad \lambda_0 = (d_A + m d_B)^{-1} \ (m = \mu_A/\mu_B).$$

To the lowest order, the kinematic equation (16) yields

$$\partial_t h_0 = -(\sigma_0 + i q_y V_{B0}) h_0 + \phi^B_{z0}(d_A),$$

where $V_{B0} = V_B^{(0)}(z = d_A) = \lambda_0 d_A \gamma \cos t$. From Eqs. (25) and (35), $\phi^B_{z0}(d_A)$ can be expressed as

$$\phi^B_{z0}(d_A) = [f^B_{z0,1}(q_x, q_y)\Gamma_0 + f^B_{z0,2}(q_x, q_y)(\partial_z V_B)_0] h_0, \tag{37}$$

with $f^B_{z0,1}$ and $f^B_{z0,2}$ complicated but known functions of wave numbers q_x and q_y (and also dependent on parameters α_1, α_{56}, and d_A), and hence,

$$\partial_t h_0 = [-\sigma_0 + f^B_{z0,1}(q_x, q_y)\Gamma_0] h_0 + [-i q_y V_{B0} + f^B_{z0,2}(q_x, q_y)(\partial_z V_B)_0] h_0. \tag{38}$$

The requirement of periodicity of h_0 with time t gives the zeroth order Floquet exponent [note that terms proportional to V_{B0} and $(\partial_z V_B)_0$ are periodic in t],

$$\sigma_0 = f^B_{z0,1}(q_x, q_y)\Gamma_0. \tag{39}$$

Consequently, with initial value $h_0(0)$,

$$h_0(t) = h_0(0) \exp\left\{ \int dt [-i q_y V_{B0} + f^B_{z0,2}(\partial_z V_B)_0] \right\} = h_0(0) \exp[(-i q_y d_A + m f^B_{z0,2}) \lambda_0 \gamma \sin t], \tag{40}$$

and the velocity fields are obtained from Eqs. (23), (25)–(28), and (35), all proportional to $h_0(t)$.

2. $\mathbf{Re} \ll 1$, $\Gamma' \ll 1$, *such that* $\Gamma'/\mathbf{Re} = \Gamma_1 = \mathcal{O}(1)$

In this case, the results of first order expansion need to be addressed. When $q_x \neq 0$, the solution to $\mathcal{O}(\mathrm{Re})$ yields

$$\phi^B_{z1} = \sum_{i=1}^{4} [B^{(1)}_i e^{b_i z} + B'_i z e^{b_i z} + B'_{i+4} z^2 e^{b_i z}], \tag{41}$$

$$\phi^B_{x1} = \sum_{i=1}^{4} C^{(1)}_i e^{r_i z} + \frac{iq_x}{q^2}\partial_z \phi^B_{z1} + \sum_{i=1}^{4} C'_i z e^{r_i z} + \sum_{i=3}^{4} C'_{i+2} z^2 e^{r_i z} + \sum_{i=1}^{4} B''_i e^{b_i z}, \tag{42}$$

$$\phi^A_{z1} = \sum_{i=1}^{4} [A^{(1)}_i e^{a_i z} + D^{(1)}_i A'_i e^{s_i z} + A'''_i z e^{a_i z}] + \sum_{i=3}^{4} A'''_{i+2} z^2 e^{a_i z} + \sum_{i=1}^{4} [D''_i e^{s_i z} + D''_{i+4} z e^{s_i z} + D''_{i+8} z^2 e^{s_i z}] \tag{43}$$

$$\phi^A_{x1} = \sum_{i=1}^{4} [D^{(1)}_i e^{s_i z} + D'_i z e^{s_i z} + D'_{i+4} z^2 e^{s_i z} + A''_i e^{a_i z}], \tag{44}$$

while for $q_x = 0$, we get $\phi^A_{x1} = \phi^B_{x1} = 0$, ϕ^B_{z1} given by Eq. (41), and

$$\phi^A_{z1} = (A^{(1)}_1 + A^{(1)}_2 z)e^{qz} + (-A^{(1)}_1 + A^{(1)}_3 z)e^{-qz} + (A'''_1 z^2 + A'''_2 z^3)e^{qz} + (A'''_3 z^2 + A'''_4 z^3)e^{-qz}. \tag{45}$$

Here exponents b_i, r_i, a_i, s_i and coefficients A'_i are the same as those in Eqs. (29)–(33), and coefficients B'_i, B''_i, C'_i, A'_i, A''_i, A'''_i, D'_i, and D''_i are complicated functions of zeroth order solutions $(A^{(0)}, B^{(0)}, C^{(0)}, D^{(0)})$. The unknown first order coefficients $(A^{(1)}, B^{(1)}, C^{(1)}, D^{(1)})$ can be determined by boundary conditions (22) and interfacial conditions (11)–(14), as in the above zeroth order case. Similar to Eq. (35), the linear matrix equation governing first order coefficients $\boldsymbol{A}^{(1)}$ $(=[A^{(1)}_j, B^{(1)}_j, C^{(1)}_j, D^{(1)}_j]$ for $q_x \neq 0$, or $[A^{(1)}_j, B^{(1)}_j]$ for $q_x = 0$, with $j = 1, 2)$ is

$$\boldsymbol{\chi} \cdot \boldsymbol{A}^{(1)} = \boldsymbol{h}^{(1)} h_0 + \boldsymbol{h}^{(0)} h_1, \tag{46}$$

with matrices $\boldsymbol{\chi}$ and $\boldsymbol{h}^{(0)}$ the same as those in Eq. (35), $h_1(t)$ as the first order interface perturbation, and the matrix $\boldsymbol{h}^{(1)}$ as a complicated function of Γ_1, $(\partial_z V_B)_0$, and $\partial_t(\partial_z V_B)_0$. Thus, the solution of Eq. (46) takes the form

$$\boldsymbol{A}^{(1)} = [\boldsymbol{\chi}^{-1}\boldsymbol{h}^{(1)}]h_0 + [\boldsymbol{A}^{(0)}/h_0]h_1, \tag{47}$$

with $\boldsymbol{A}^{(0)}$ given by Eq. (35), and accordingly the first order velocity fields can be calculated with the use of Eqs. (41)–(45).

The $\mathcal{O}(\mathrm{Re})$ result of the kinematic condition (16) is given by

$$\partial_t h_1 = -(\sigma_0 + iq_y V_{B0})h_1 - (\sigma_1 + iq_y V_{B1})h_0 + \phi^B_{z1}(d_A), \tag{48}$$

where $V_{B1} = \lambda_2 \gamma \sin t$ is the first order base flow $V^{(1)}_B$ evaluated at interface $z = d_A$, with

$$\lambda_2 = \tfrac{1}{2}(\lambda_1 d_A - \lambda_0 d_A^3/3), \quad \lambda_1 = [(d_A^3 + m^2 d_B^3)/3 + m d_A d_B d]\lambda_0^2.$$

The value of $\phi^B_{z1}(d_A)$ is determined by solution (41), and from Eq. (47) we find

$$\phi^B_{z1}(d_A) = [f^B_{z1,1}(q_x, q_y)\Gamma_1 + f^B_{z1,2}(q_x, q_y)(\partial_z V_B)_0 + f^B_{z1,3}(q_x, q_y)(\partial_z V_B)_0^2 + f^B_{z1,4}(q_x, q_y)\partial_t(\partial_z V_B)_0]h_0 + [\phi^B_{z0}(d_A)/h_0]h_1, \tag{49}$$

with $\phi^B_{z0}(d_A)$ the zeroth order solution as in Eq. (37), $f^B_{z1,1} = f^B_{z0,1}$, and $f^B_{z1,i}$ $(i = 2, 3, 4)$

obtained from first order solution (47) and functions of α_1, α_{56}, and d_A. Substituting Eqs. (49), (36), and (39) into (48), and using the condition that h_1 is periodic in time, we obtain the first order Floquet exponent

$$\sigma_1 = f^B_{z1,1}(q_x,q_y)\Gamma_1 + \tfrac{1}{2}\delta^2\gamma^2 f^B_{z1,3}(q_x,q_y), \tag{50}$$

and the corresponding interface perturbation

$$h_1(t) = [h_1(0)/h_0(0) + f^B_{z1,2}\delta\gamma \sin t + f^B_{z1,3}\delta^2\gamma^2(\sin 2t)/4 - (iq_y\lambda_2 + \delta f^B_{z1,4})\gamma(1-\cos t)]h_0(t), \tag{51}$$

with $h_0(t)$ given in Eq. (40). [It is convenient to choose $h_1(0)=0$ at time $t=0$ so that the initial condition for h is $h(t=0)=h_0(0)$, independent of Re.]

Equation (50) determines stability. The first term of the right-hand side is proportional to rescaled surface tension and is always negative, indicating the stabilizing effect of surface tension. The second term, proportional to γ^2, incorporates the effect of the imposed shear flow and tends to destabilize the planar boundary. Detailed results are shown in the next section.

IV. RESULTS

Given the results of the previous section, the stability of the boundary depends on the two viscosity coefficients α_1 and α_{56}, on the domain thickness d_A, the shear strain γ, as well as the Reynolds number Re and the rescaled surface tension Γ' (both ω dependent). Here we focus on three characteristic regimes of Γ' (all with $\mathrm{Re}\ll 1$ as appropriate for typical copolymers): $\Gamma'=\mathcal{O}(1)$, $\Gamma'/\mathrm{Re}=\mathcal{O}(1)$, and $\Gamma'/\mathrm{Re}\ll 1$, corresponding to different ranges of shear frequencies.

A. $\mathrm{Re}\to 0$ and $\Gamma'=\mathcal{O}(1)$

The first regime of interest is that of very small Reynolds number ($\mathrm{Re}\to 0$) and finite surface tension [$\Gamma'=\Gamma_0=\mathcal{O}(1)$], which corresponds to very low frequency ω according to the analysis at the beginning of Sec. III C. The Floquet exponent (or the perturbation growth rate) is then well approximated by zeroth order result σ_0 in Eq. (39). Our calculations give $\sigma_0 \leqslant 0$ [i.e., $f^B_{z0,1}(q_x,q_y)\leqslant 0$] for all wave numbers q_x and q_y; thus, the system is always stable, resulting in the coexistence of parallel and perpendicular domains under shear flow. The stabilizing effect of surface tension dominates, and $\sigma_0 \propto \Gamma_0$ as shown in Eq. (39).

B. $\mathrm{Re}\ll 1$, $\Gamma'\ll 1$, and $\Gamma'/\mathrm{Re}=\mathcal{O}(1)$

In an intermediate range of ω, Γ' is of order $\mathcal{O}(\mathrm{Re})$ as discussed in Sec. III C. The perturbation growth rate can be written as $\sigma=\mathrm{Re}\,\sigma_1$ with the first order exponent σ_1 given in Eq. (50). Note that $f^B_{z1,1}=f^B_{z0,1}\leqslant 0$ whereas the maximum value of $f^B_{z1,3}$ can be positive depending on system parameters α_1, α_{56}, and d_A, leading to a competition between the stabilizing effect of surface tension (proportional to $\Gamma_1=\Gamma'/\mathrm{Re}$) and the destabilizing influence of the imposed shear (proportional to γ^2). Note that Γ_1 can also be expressed from Eqs. (15) and (3) as

$$\Gamma_1 = 1/\mathrm{We} = [\Gamma/(\rho d^3)]\omega^{-2} \equiv \theta\omega^{-2}, \tag{52}$$

with We as the Weber number and $\theta=\Gamma/(\rho d^3)$. Thus, a system would be more unstable for larger shear strain γ and frequency ω.

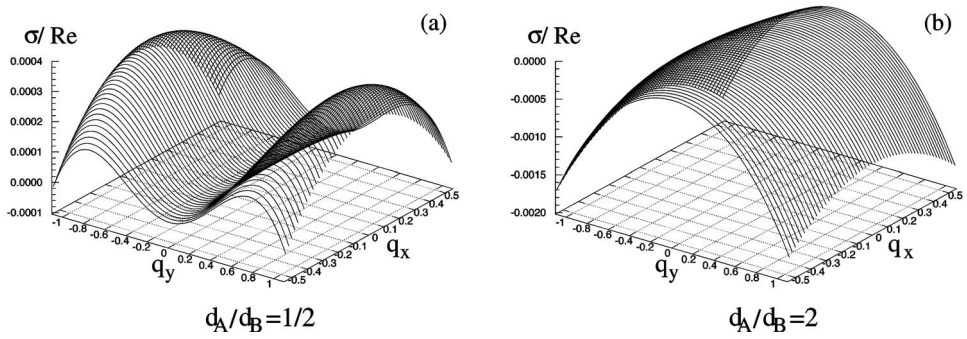

FIG. 3. Growth rate σ/Re as a function of wave numbers q_x and q_y, for $\alpha_1=1$, $\alpha_{56}=-0.9$, $\gamma=1$, $\mathrm{Re}=5\times10^{-4}$, as well as (a) $d_A=1/3$ (with $d_A/d_B=1/2$), with maximum growth rate $\sigma_{\max}=3.4\times10^{-4}$ Re found at $q^{\max}=(0,\pm0.89)$, and (b) $d_A=2/3$ (with $d_A/d_B=2$), indicating that $\sigma\leqslant0$ at all wave vectors.

To examine the onset of instability, we have carried out a numerical evaluation of σ for a range of typical system parameters. For a typical copolymer system, $\rho=1$ g cm^{-3}, $\Gamma=1$ dyn/cm, $\eta=10^4$ P, and $d=1$ cm, with Reynolds number $\mathrm{Re}=(10^{-4}\ \mathrm{s})\omega$ and rescaled surface tension $\Gamma'=(10^{-4}\ \mathrm{s}^{-1})/\omega$. The two dimensionless viscosities are set as: $\alpha_1=1$, and $\alpha_{56}=-0.9$ (corresponding to an effective viscosity $\mu_B=1/10$ and thus a ratio $m=\mu_A/\mu_B=10$) or $\alpha_{56}=9$ (corresponding to $\mu_B=10$ and $m=1/10$).

Figure 3 shows the growth rate $\sigma_1=\sigma/\mathrm{Re}$ as a function of wave numbers (q_x,q_y), for $\alpha_{56}=-0.9$ and two different domain thicknesses $d_A=1/3$ (with $d_A/d_B=1/2$) and $2/3$ (with $d_A/d_B=2$). The most dangerous wave numbers are near $q_x=0$, as can be seen in Fig. 3(a). The figure shows that the maximum growth rate ($\sigma_{\max}=3.4\times10^{-4}\mathrm{Re}$) occurs at $q_x^{\max}=0$ and $q_y^{\max}=\pm0.89$. Results for the larger ratio $d_A/d_B=2$ are shown in Fig. 3(b), indicating that the system is stable. When $\alpha_{56}=9$, we obtain opposite stability results: a small ratio $d_A/d_B=1/2$ corresponds to a stable configuration, whereas instability occurs for $d_A/d_B=2$, with $\sigma_{\max}$ also found at $q_x=0$. It is also interesting to note that at $d_A/d_B=1$, instability occurs for all values of α_{56} (i.e., for all effective viscosity contrast). Figure 4 shows the maximum growth rate for $\gamma=1$ and 0.5, $\omega=5$ and 10 (s^{-1}) (corresponding to

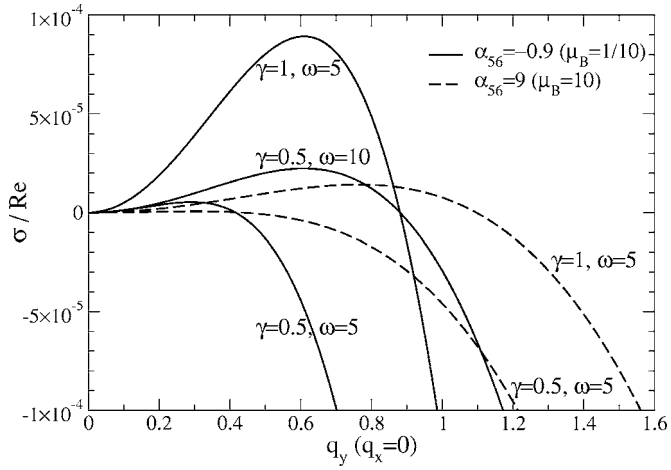

FIG. 4. Growth rate σ/Re versus q_y at $q_x=0$ for $d_A/d_B=1$ and different values of γ, ω, and α_{56}.

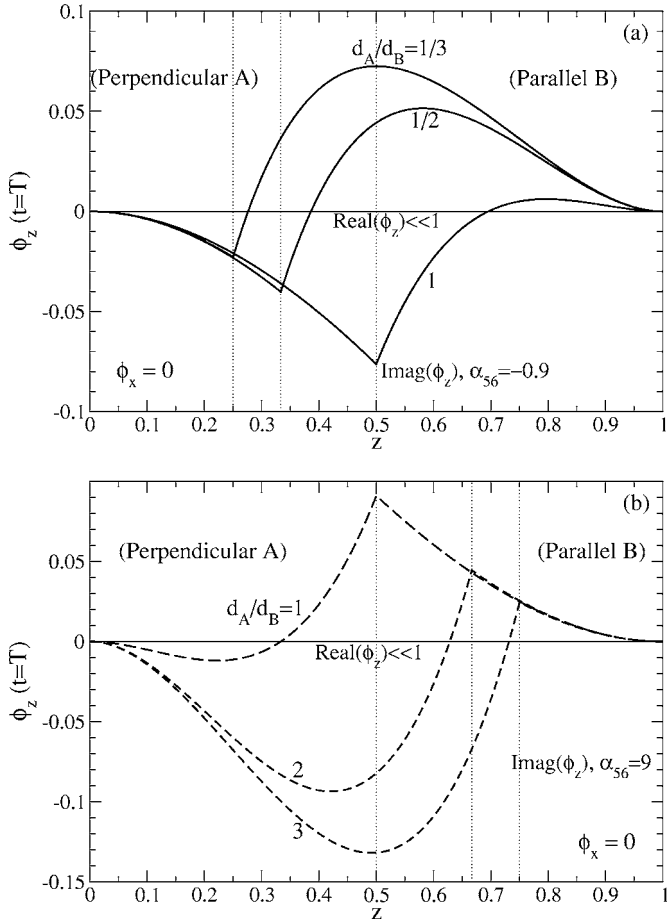

FIG. 5. Spatial dependence of the velocity amplitude ϕ_z at time $t=T$ $(=2\pi)$, at the most unstable wave vectors $(q_x^{\max}=0, q_y^{\max})$ given by Figs. 3 and 4. All the curves here correspond to unstable configuration with $\sigma>0$, with parameters $\mathrm{Re}=5\times10^{-4}$, $\alpha_1=1$, and $\gamma=1$. (a) $\alpha_{56}=-0.9$ $(\mu_B=1/10)$, for $d_A/d_B=1$, 1/2, and 1/3; (b) $\alpha_{56}=9$ $(\mu_B=10)$, for $d_A/d_B=1$, 2, and 3. The locations of domain interface are indicated by dotted lines.

$\mathrm{Re}=5\times10^{-4}$ and 10^{-3}), and two different viscosities $\alpha_{56}=-0.9$ and 9. As the shear strain amplitude γ or frequency ω decreases, the range of unstable wave numbers also decreases. This observation motivates the analysis of long wave solutions presented in Sec. IV D.

The perturbed velocity fields are defined by Eq. (23). The velocity associated with the most unstable wave vector $(q_x=0, q_y\neq0)$ is given by

$$\hat{u}_x^{\max}=0 \quad \text{and} \quad \hat{u}_z^{\max}=\phi_z\exp(\sigma_{\max}t),$$

with ϕ_z determined by Eqs. (25), (34), (41), and (45). Results for ϕ_z at the most unstable wave numbers are shown in Fig. 5 (at $t=T$), and in Fig. 6 (at the interface $z=d_A$), for $\alpha_1=1$, $\gamma=1$, $\mathrm{Re}=5\times10^{-4}$ (with $\omega=5\ \mathrm{s}^{-1}$), as well as for a variety of domain thickness ratios d_A/d_B and different viscosity coefficients $\alpha_{56}=-0.9$ and 9. The corresponding interfacial perturbation $h(t)$, defined in Eq. (23), is shown in Fig. 7. Although the velocity fields near the interface are sensitive to the viscosity contrast and thickness ratios [e.g., the temporal dependence of ϕ_z for $\mu_B=1/10$ (with $\alpha_{56}=-0.9$) and $\mu_B=10$ $(\alpha_{56}=9)$ is out

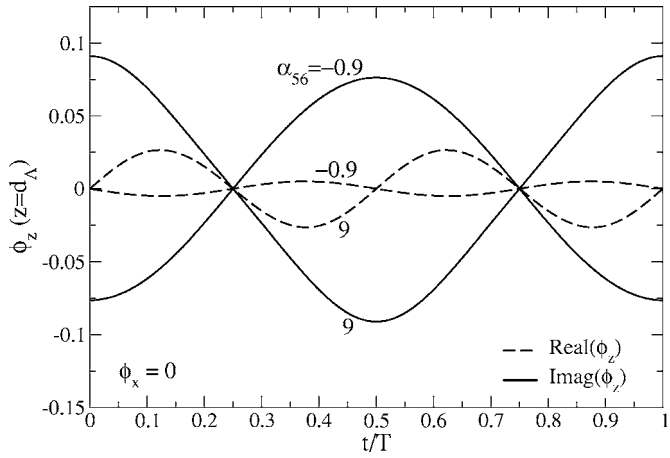

FIG. 6. Temporal dependence of the velocity amplitude ϕ_z over a period T at the interface $z=d_A$, with $d_A/d_B=1$, and other parameters the same as those of Fig. 5.

of phase at the interface, as shown in Fig. 6], the qualitative results are the same: The instability develops around the interface, and relaxes into the perpendicular (A) and parallel (B) bulk regions. Importantly, the perturbation flow is directed along the z direction (and y, due to the incompressibility condition), and hence, it is transverse to the parallel lamellae. If the monomer density order parameter were allowed to diffuse, this secondary flow would result in the distortion of parallel lamellae, but not perpendicular.

C. Re≪1 and Γ′/Re≪1

In the limit $\Gamma'/\mathrm{Re}\ll 1$, which corresponds to small surface tension Γ or large enough ω, the effect of the surface tension is negligible at least for solutions up to first order. This leads to $\Gamma_0=\Gamma_1=0$ in the solutions of Sec. III. Thus $\sigma_0=0$, and according to Eq. (50) the first order growth rate is

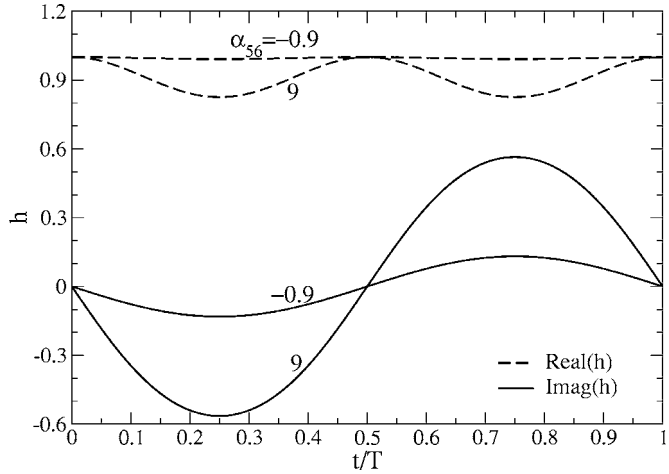

FIG. 7. Temporal dependence of the interface perturbation h over a period T, with parameters the same as those of Fig. 6.

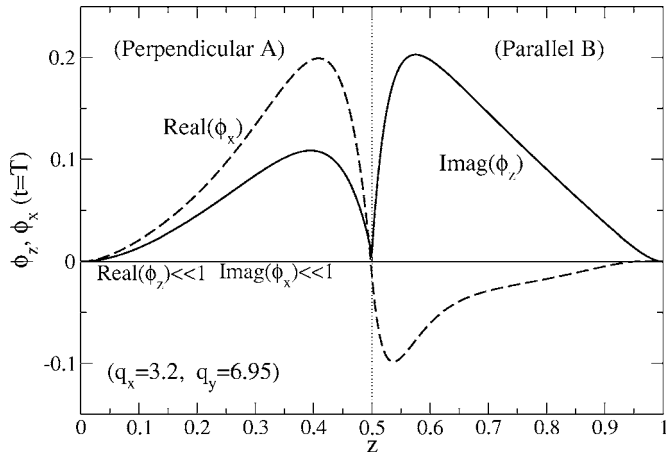

FIG. 8. Velocity amplitudes ϕ_x and ϕ_z (at time $t=T$) as a function of position z, at the most unstable wave numbers $(q_x^{\max}, q_y^{\max})=(3.2, 6.95)$. The parameters are chosen as $\alpha_{56}=-0.9$, $d_A/d_B=1$, $\gamma=1$, and $\mathrm{Re}=10^{-2}$ (corresponding to large $\omega=100\ \mathrm{s}^{-1}$).

$$\sigma_1 = \tfrac{1}{2}\delta^2\gamma^2 f^B_{z1,3}(q_x, q_y). \tag{53}$$

The function $f^B_{z1,3}(q_x, q_y)$ can be positive, and note that it is independent of shear parameters γ and ω. The growth rate is proportional to γ^2.

A typical profile for the velocity functions ϕ_x and ϕ_z is shown in Fig. 8. In contrast with the regime discussed in Sec. IV B $[\Gamma'/\mathrm{Re}=\Gamma_1=\mathcal{O}(1)]$, the most unstable wave numbers $q_x^{\max}$ and $q_y^{\max}$ here are both nonzero. As shown in Fig. 8 and unlike the limit discussed in Sec. IV B, perturbed velocity fields develop along both x and z directions (i.e., $\phi_x, \phi_z \neq 0$), leading to the distortion of both parallel and perpendicular regions. Therefore, although the parallel/perpendicular interface will move in response to the hydrodynamic instability and the resulting secondary flows, the direction of motion and, hence, the dominant lamellar orientation cannot be deduced from this analysis.

D. Long wave solutions

The calculations presented so far show that in the limit $\mathrm{Re} \ll 1$, $\Gamma' \ll 1$, with $\Gamma'/\mathrm{Re} = \mathcal{O}(1)$, the wave numbers associated with instability lie at $q_x=0$ and small q_y, as seen in Fig. 3. Thus, we discuss next a long wave approximation to the stability analysis. We expand the solutions of Sec. III C in powers of q $(=q_y$ here), and find that

$$f^B_{z1,1} = f^B_{z0,1} = -f_0 q^4 + \mathcal{O}(q^6), \tag{54}$$

with

$$f_0 = \frac{1}{3\Delta} d_A^3 d_B^3 (1 + \alpha_{56} d_A) > 0, \tag{55}$$

and

$$f^B_{z1,3} = f_1 q^2 + f_2 q^4 + \mathcal{O}(q^6), \tag{56}$$

where

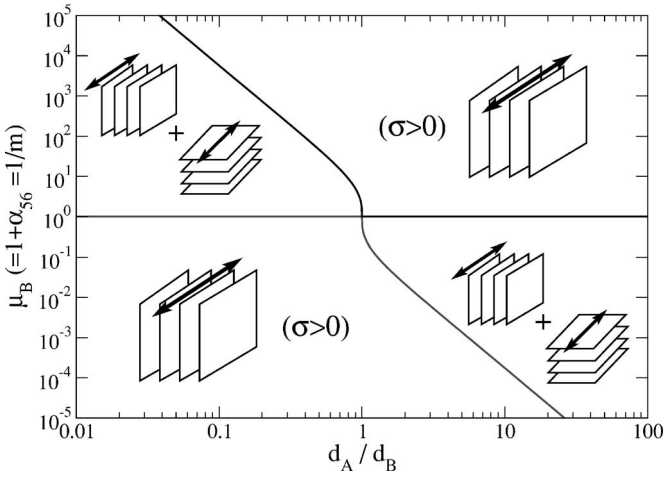

FIG. 9. Stability diagram of thickness ratio d_A/d_B versus viscosity contrast μ_B ($=m^{-1}$). For the unstable regime with $\sigma>0$, the perpendicular phase is selected over the parallel one, while the stability leads to the coexistence of parallel and perpendicular orientations.

$$f_1 = \frac{1}{60\Delta^3} d_A^2 d_B^2 \alpha_{56} f_{11} f_{12}, \tag{57}$$

with

$$\begin{aligned} f_{11} &= (1+\alpha_{56}d_A^2)^2 + 4\alpha_{56}d_A^2 d_B(1+\alpha_{56}d_A) > 0, \\ f_{12} &= (d_A-d_B)(d_A^2+d_B^2) + d_A^8\alpha_{56}^4 + 2d_A^5[d_A d_B^2 + 2(d_A-d_B)]\alpha_{56}^3 + 2d_A^2[3(d_A-d_B)^2 \\ &\quad + (1-d_A^2)^2 - 2d_B^3(1+d_B)^2]\alpha_{56}^2 + 2d_A[2(d_A-d_B)^2 + 3d_A d_B^2 - 4(1+d_A)d_B^4]\alpha_{56}, \end{aligned} \tag{58}$$

and f_2 a complicated but known function of d_A, α_1, and α_{56}. Here Δ is defined as

$$\Delta = (d_B^2 - \mu_B d_A^2)^2 + 4\mu_B d_A d_B > 0. \tag{59}$$

Therefore, the first order Floquet exponent (50) can be rewritten as

$$\sigma_1 = \theta f_{z1,1}^B \omega^{-2} + \tfrac{1}{2}\delta^2 f_{z1,3}^B \gamma^2 = \tfrac{1}{2}\delta^2 f_1 \gamma^2 q^2 - \left(\theta f_0 \omega^{-2} - \tfrac{1}{2}\delta^2 f_2 \gamma^2\right) q^4. \tag{60}$$

Thus, when $f_1>0$ at small q we have $\sigma_1>0$ for all γ and ω. From the definition of f_1, we note that stability is determined by the sign of $\alpha_{56}f_{12}$ [Eqs. (57) and (58)] which is itself a function of α_{56} and d_A only, and independent of shear parameters γ and ω. The calculated stability diagram of d_A/d_B vs μ_B ($=1+\alpha_{56}$) is shown in Fig. 9. The diagram is symmetric with respect to $d_A/d_B \to (d_A/d_B)^{-1}$ and $\mu_B \to \mu_B^{-1}$. [Note that at $d_A/d_B=1$ (i.e., $d_A=1/2$) instability is found for all values of μ_B, in agreement with the numerical results in Sec. IV B.] This diagram reveals the analog of the thin layer effect in the interfacial instability caused by viscosity stratification of two superposed Newtonian fluids [Hooper (1985)]. When the thinner domain has the larger effective viscosity, instability occurs. Unlike the Newtonian case, here the effective viscosity contrast is caused by the orientation dependence of the dissipative part of the stress tensor. Note the for a polycrystalline sample, although the value of α_{56} (μ_B) would be determined by the specific copolymer considered, the thickness ratio d_A/d_B would vary from domain to domain. Thus,

according to Fig. 9, the development of the instability would differ in different portions of a large sample.

The largest perturbation growth rate can be obtained from Eq. (60). When $\theta f_0 \omega^{-2} - 1/2\,\delta^2 f_2 \gamma^2 > 0$, or

$$\gamma^2 \omega^2 < \frac{2\theta f_0}{\delta^2 f_2}, \tag{61}$$

we obtain

$$\begin{aligned} \sigma_1^{\max} &= \frac{\delta^4 f_1^2}{16(\theta f_0 - \delta^2 f_2 \gamma^2 \omega^2/2)} \gamma^4 \omega^2, \\ q_{\max} &= \frac{1}{2}\delta \left(\frac{f_1}{\theta f_0 - \delta^2 f_2 \gamma^2 \omega^2/2} \right)^{1/2} \gamma\omega. \end{aligned} \tag{62}$$

These formulae show that both maximum growth rate and most unstable wave number increase with shear amplitude γ and frequency ω, in agreement with the numerical results of Sec. IV B and Fig. 4.

V. DISCUSSION

The analysis given is purely of hydrodynamic nature and makes no reference to the response of the lamellar phases to the flows considered. The fully coupled problem is very complex, but the flow analysis conducted here can be used to argue indirectly about orientation selection. The flow perturbation $\mathbf{u}$ will advect the lamellae through the advection term $\mathbf{u}\cdot\nabla\psi$ in Eq. (1), with ψ the monomer concentration. Parallel lamellae are marginal to velocity fields along the x and y directions since these flows are parallel to the planes of constant ψ, but will be distorted by flows in the z direction (Fig. 2). Conversely, perpendicular lamellae are unaffected by flows along either z or y, but distorted by those along the x direction. The instability mode given in Sec. IV B for $\Gamma'/\mathrm{Re} = \mathcal{O}(1)$ which might be of most experimental relevance {if we estimate the order of surface tension Γ from the grain boundary interfacial energy [Matsen (1997); Netz *et al.* (1997)], as discussed in Sec. III C} and hence is our focus here, is associated with secondary flows with $u_x = 0$ and $u_z \neq 0$; thus parallel lamellae are compressed or expanded, while the lamellar configuration in the perpendicular region remains unaffected due to the absence of modulation along its normal. Distortion of parallel lamellae would create a relative imbalance of free energy $\mathcal{F}$ in the two domains: $\mathcal{F}_{\mathrm{Parallel}} > \mathcal{F}_{\mathrm{Perpendicular}}$. This free energy imbalance would be relieved through the motion of the domain boundary towards the distorted parallel region. Therefore we would anticipate that a consequence of the shear flow and the resulting interfacial instabilities would be the growth of the perpendicular region at the expense of the parallel one.

Therefore, the stability diagram of Fig. 9 can be used to indirectly address orientation selection, suggesting coexistence of parallel and perpendicular domains (in the hydrodynamically stable regime) or the selection of the perpendicular orientation (in the unstable regime). It would be interesting to examine an experimental system composed of only two domains of parallel and perpendicular orientations, for verifying our predictions such as the change of instability with domain thickness ratio d_A/d_B and viscosity contrast μ_B, measuring the viscosity contrast from the location of the instability boundary, and further studying the domain evolution beyond the instability stage.

Polycrystalline samples of the type present in all shear aligning experiments involve a distribution of grain sizes and orientations. We address next how the results just obtained may provide a criterion for orientation selection under certain circumstances. Experiments [Gido *et al.* (1993); Qiao and Winey (2000)] reveal the presence of grain boundaries separating domains of different orientations, and we argue that the motion of these grain boundaries under the imposed shear affects the selection process. This mechanism is different than other suggestions in the literature involving grain rotation, domain instabilities, or other effects of microscopic origin that are related to block architecture (looping and bridging) [Wu *et al.* (2004); Wu *et al.* (2005)].

Earlier research has shown that boundaries of domains with a lamellar normal that has a component along the transverse direction will move, leading to a decrease in the size of the domain. The shear increases the free energy density of the transverse domain and originates diffusive monomer redistribution at the boundary to reduce the extent of the phase of higher free energy [Huang *et al.* (2003); Huang and Viñals (2004)]. Since the free energy of neither parallel nor perpendicular lamellae is affected by the shear (at least in the low frequency range of $\omega \ll \omega_c$ in which the Leibler [Leibler (1980)] or Ohta–Kawasaki [Ohta and Kawasaki (1986)] free energies are a good approximation), one can generally expect grain boundaries to move toward the transverse phase. Our interest in this paper is therefore in possible physical mechanisms that would account for the motion of boundaries separating domains of parallel and perpendicular orientations. According to Fig. 9, if $\alpha_{56} > 0$ (as might be appropriate, for example, for PEP-PEE diblocks) an initially large perpendicular domain (A) adjacent to a smaller parallel domain (B) (so that d_A/d_B is large) would grow even larger. Although our analysis does not hold beyond the linear stage of boundary deformation, it seems unlikely that any nonlinearity could saturate boundary distortion and lead to a stationary but corrugated boundary. Therefore we would predict that the perpendicular orientation will be selected for $\alpha_{56} > 0$. If, on the other hand, $\alpha_{56} < 0$ (as would be appropriate, for example, for PS-PI diblocks), the situation is more complicated. Instability now occurs for d_A/d_B small, leading to growth of the perpendicular domain and, hence, to an increase of the characteristic scale d_A. To the extent that, in a sufficiently large system the boundary remains quasi planar, the stability boundary in Fig. 9 would be reached. Once inside the stable region, any remaining curved boundaries would be expected to relax to planarity (driven by excess free energy reduction), as the planar boundary would no longer be unstable under shear. Therefore, in the case of $\alpha_{56} < 0$, we would anticipate coexistence of parallel and perpendicular domains, or perhaps a dependence of the selected orientation on initial condition or sample history.

We finally examine the dependence of the largest growth rate $\sigma_{\max}$ on the shear amplitude γ and angular frequency ω near the onset of instability. Note that the stability boundaries of Fig. 9 are independent of both parameters, but near onset where $\sigma \sim \mathcal{O}(\mathrm{Re}) \ll 1$, experiments might detect an effective stability boundary located at the point on which $1/\sigma_{\max}$ is of the order of the observation time of the experiment. From Eq. (3) we have

$$\sigma_1^{\max} = \sigma_{\max}/\mathrm{Re} = \sigma_{\max}\,\eta/(\rho d^2 \omega),$$

and then given Eq. (62) we find that

$$\gamma^2\omega^2\left(\gamma^2\omega + \frac{8 f_2 \eta \sigma_{\max}}{\delta^2 f_1^2 \rho d^2}\right) = \frac{16\theta f_0 \eta \sigma_{\max}}{\delta^4 f_1^2 \rho d^2}, \tag{63}$$

with associated wave number

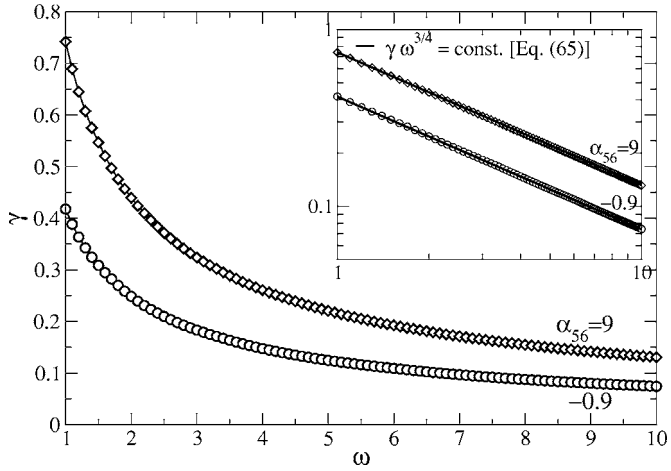

FIG. 10. Lines of constant $\sigma_{\max}$ ($=10^{-11}$) for $d_A/d_B=1$. Symbols (circles and diamonds) are from numerical calculations, while the solid lines in the inset follow the scaling given by the long wave approximation in Eq. (65), that is, $\gamma\omega^{3/4}=$const.

$$q_{\max}=\left(\frac{\eta\sigma_{\max}}{\theta f_0\rho d^2}\right)^{1/4}\omega^{1/4}. \tag{64}$$

Usually $\gamma^2\omega \gg 8|f_2|\,\eta\sigma_{\max}/(\delta^2 f_1^2\rho d^2)$ for very small value of $\sigma_{\max}$, and thus we obtain

$$\sigma_{\max}=\frac{\rho d^2\delta^4 f_1^2}{16\theta f_0\eta}\gamma^4\omega^3, \tag{65}$$

which scales as $\gamma\omega^{3/4}$ for a given block copolymer. Therefore, the line of constant $\sigma_{\max}$ is given by $\gamma\omega^{3/4}=$const. This result is consistent with our numerical evaluation of solutions in Sec. III C 2, as shown in Fig. 10 for two cases of $\alpha_{56}=-0.9$ (circles) and 9 (diamonds). Note that the data in the log-log plot of the inset is well fitted to a straight line with slope $-3/4$. For small enough $\sigma_{\max}$ (e.g., $=10^{-11}$ as in Fig. 10), which is the order of the inverse experimental observation time, this line can correspond to an effective stability boundary above which the instability becomes experimentally observable.

To our knowledge, the only experimental determination in γ-ω space of the regions in which parallel or perpendicular lamellae are selected has been carried out for PS-PI block copolymers [Maring and Wiesner (1997); Leist *et al.* (1999)]. It has been found that the line separating regions of perpendicular and parallel orientations was approximately given by $\gamma\omega=$const. No results for copolymers with $\alpha_{56}>0$ (such as PEP-PEE) are available. Given that our predictions of effective boundary only apply to this case, it would be of interest to repeat the experiments for this type of copolymers.

The above discussion corresponds to a range of shear frequency so that $\Gamma'/\mathrm{Re}=\mathcal{O}(1)$. For very low frequencies so that $\mathrm{Re}\to 0$ while $\Gamma'=\mathcal{O}(1)$, a parallel/perpendicular configuration is always stable due to the dominant effect of surface tension (as given in Sec. IV A).

In combination with the stability of the lowest frequencies, our results in Fig. 10 indicate that the perpendicular orientation would be observed for large enough ω and γ. Otherwise, both parallel and perpendicular lamellae would coexist, and the selection between them would depend on experimental details such as quenched or annealed his-

tory of the sample and the starting time of the shear, as found in PS-PI copolymer samples [Patel *et al.* (1995); Maring and Wiesner (1997); Larson (1999)] and cannot be addressed by the stability analysis here.

We have adopted an important simplification in the analysis above, namely that hydrodynamic flow and elastic copolymer response to lamellar distortion can be decoupled in the configuration examined. Within the mesoscopic description of Leibler [Leibler (1980)] and Ohta/Kawasaki [Ohta and Kawasaki (1986)] that we have followed, the decoupling results from the fact that at leading order $\mathbf{v}\cdot\boldsymbol{\nabla}\psi=0$ throughout the entire system for the particular parallel/perpendicular configuration studied. It is known, however, that even in the parallel or perpendicular configurations entanglement effects can lead to normal stresses at finite frequencies, to lamellar wavelength reduction, and to possible undulational instabilities [Williams and MacKintosh (1994)]. These effects are completely absent in this description, consistent with its assumption that the frequencies examined are low compared with inverse chain relaxation times.

Even within the mesoscopic-scale and low-frequency description employed, flow and elastic copolymer response are generally coupled when lamellar normals have a projection along the transverse direction. The resulting elastic effects have been addressed by Amundson and Helfand (1993) and Wang (1994) concerning mechanical properties and instabilities, and by Drolet *et al.* (1999) and Huang *et al.* (2003) concerning the response to oscillatory shears. In particular, Huang *et al.* (2003) showed that a boundary separating parallel and transverse orientations always moves towards the transverse region when sheared precisely because of the extra elastic energy stored in that region. A similar argument can be made for boundaries separating transverse and perpendicular lamellae. These analyses, however, cannot discriminate between parallel and perpendicular regions, as both are marginal with respect to the shear within the mesoscopic description adopted. Given that experiments addressing shear induced ordering usually concern parallel and perpendicular orientations and transitions between the two, and that those transitions are observed in a range of low shear frequencies for which the mesoscopic models of Leibler and Ohta/Kawasaki should be applicable, we have focused on a possible mechanism than can contribute to orientation selection *absent* elastic effects. Extension of our results to finite frequencies is currently under way.

Further extension of our study would involve the examination of domain coarsening beyond the initial instability stage, particularly the role of nonlinearities on system evolution, or the effect of domain correlations and competition in a poly domain sample. This would involve the numerical solution of the coupled order parameter (i.e., the copolymer concentration field) dynamics and the hydrodynamic Eq. (2) with the constitutive law, as described at the beginning of Sec. II A. Previous efforts involving direct numerical simulations of block copolymer ordering that allow for hydrodynamic coupling are limited [Maurits *et al.* (1998); Xu *et al.* (2005); Hall *et al.* (2006)]. In addition, the interpretation of the results is further complicated by the small aspect ratio of the systems employed in the simulations (the aspect ratio is the ratio between the lateral dimension of the system and the lamellar wavelength). The constitutive law that we have introduced for the dissipative stress tensor will further complicate any numerical treatment. In fact, it is likely that in order to address large enough aspect ratios, simulations of simplified, two domain configuration analogous to that studied here (Fig. 2) would be a good starting point for our understanding of orientation selection in polycrystalline samples.

VI. SUMMARY

The assumption of a dissipative part of the stress tensor σ^D_{ij} which is compatible with the uniaxial symmetry of a lamellar phase leads to an effective dynamic viscosity that

depends on the orientation of the lamellae relative to the shear. We expect this functional form of σ_{ij}^{D} to capture the low frequency and long wavelength response to the lamellar phase, without making reference to the microscopic origin of the viscosity coefficients. We have explored here the consequence of this assumption on a configuration comprising parallel and perpendicular domains. Experimental evidence suggests that these two orientations are prevalent in shear aligning experiments, and we believe that the type of rheology proposed here may contribute to our understanding of the orientation selected as a function of the parameters of the block and of the shear.

In particular, we have shown that an oscillatory shear imposed on a block copolymer configuration comprising lamellar domains of parallel and perpendicular orientations can cause instability at the domain interface. The instability manifests itself by finite wave number undulations of the velocity field along the direction normal to parallel lamellae, which we argue would ultimately result in the growth of the perpendicular region at the expense of the parallel one. Our results indicate that the instability, and the selection of the perpendicular orientation, occur at an intermediate frequency range of small but finite value of Re, and depend on both viscosity contrast and domain thickness ratio. This instability is analogous to the thin layer effect in stratified fluids; that is, the system is unstable when the thinner domain is more viscous. On the other hand, at very low frequencies ($\mathrm{Re} \to 0$), coexistence of parallel and perpendicular lamellae is found as implied by hydrodynamic stability. Also, in contrast to previous studies, the selection mechanism between parallel and perpendicular orientations introduced here is of dynamical nature, and an indirect consequence of the secondary flows generated by a hydrodynamic instability of the two domain interface. It would be interesting to check our predictions experimentally in a test configuration of block copolymers as we have discussed here. Note that the frequency range studied here is $\omega < \omega_c$ in which polymer chains remain relaxed and hence the details of the individual blocks are not important. Thus our results should be independent of number and type of blocks in a copolymer.

ACKNOWLEDGMENTS

This work has been supported by the National Science Foundation under Grant No. DMR-0100903 and by NSERC Canada.

References

Amundson, K., and E. Helfand, "Quasi-static mechanical properties of lamellar block copolymer microstructure," Macromolecules **26**, 1324 (1993).

Cates, M. E., and S. T. Milner, "Role of shear in the isotropic-to-lamellar transition," Phys. Rev. Lett. **62**, 1856 (1989).

Chen, P., and J. Viñals, "Lamellar phase stability in diblock copolymers under oscillatory shear flows," Macromolecules **35**, 4183 (2002).

Chen, Z. R., and J. A. Kornfield, "Flow-induced alignment of lamellar block copolymer melts," Polymer **39**, 4679 (1998).

de Gennes, P. G., and J. Prost, *The Physics of Liquid Crystals* (Clarendon, Oxford, 1993).

Drolet, F., P. Chen, and J. Viñals, "Lamellae alignment by shear flow in a model of a diblock copolymer," Macromolecules **32**, 8603 (1999).

Ericksen, J. L., "Anisotropic fluids," Arch. Ration. Mech. Anal. **4**, 231 (1960).

Forster, D., T. C. Lubensky, P. C. Martin, J. Swift, and P. S. Pershan, "Hydrodynamics of liquid crystals," Phys. Rev. Lett. **26**, 1016 (1971).

Fredrickson, G. H., "Steady shear alignment of block copolymers near the isotropic-lamellar transition," J. Rheol. **38**, 1045 (1994).

Fredrickson, G. H., and F. S. Bates, "Dynamics of block copolymers," Annu. Rev. Mater. Sci. **26**, 501 (1996).

Fredrickson, G. H., and E. Helfand, "Fluctuation effects in the theory of microphase separation in block copolymers," J. Chem. Phys. **87**, 697 (1987).

Gido, S. P., J. Gunther, E. L. Thomas, and D. Hoffman, "Lamellar diblock copolymer grain boundary morphology. 1. Twist boundary characterization," Macromolecules **26**, 4506 (1993).

Goulian, M., and S. T. Milner, "Shear alignment and instability of smectic phases," Phys. Rev. Lett. **74**, 1775 (1995).

Guo, H. X., "Shear-induced parallel-to-perpendicular orientation transition in the amphiphilic lamellar phase: A nonequilibrium molecular-dynamics simulation study," J. Chem. Phys. **124**, 054902 (2006).

Gupta, V. K., R. Krishnamoorti, J. A. Kornfield, and S. D. Smith, "Evolution of microstructure during shear alignment in a polystyrene-polyisoprene lamellar diblock copolymer," Macromolecules **28**, 4464 (1995).

Hall, D. M., T. Lookman, G. H. Fredrickson, and S. Banerjee, "Hydrodynamic self-consistent field theory for inhomogeneous polymer melts," Phys. Rev. Lett. **97**, 114501 (2006).

Hooper, A. P., "Long-wave instability at the interface between two viscous fluids: Thin layer effects," Phys. Fluids **28**, 1613 (1985).

Huang, Z.-F., F. Drolet, and J. Viñals, "Motion of a transverse/parallel grain boundary in a block copolymer under oscillatory shear flow," Macromolecules **36**, 9622 (2003).

Huang, Z.-F., and J. Viñals, "Shear induced grain boundary motion for lamellar phases in the weakly nonlinear regime," Phys. Rev. E **69**, 041504 (2004).

King, M. R., D. T. Leighton, Jr., and M. J. McCready, "Stability of oscillatory two-phase couette flow: theory and experiment," Phys. Fluids **11**, 833 (1999).

Koppi, K. A., M. Tirrell, F. S. Bates, K. Almdal, and R. H. Colby, "Lamellar orientation in dynamically sheared diblock copolymer melts," J. Phys. II **2**, 1941 (1992).

Larson, R. G., *The Structure and Rheology of Complex Fluids* (Oxford University Press, New York, 1999).

Larson, R. G., K. I. Winey, S. S. Patel, H. Watanabe, and R. Bruinsma, "The rheology of layered liquids: Lamellar block copolymers and smectic liquid crystals," Rheol. Acta **32**, 245 (1993).

Leibler, L., "Theory of microphase separation in block copolymers," Macromolecules **13**, 1602 (1980).

Leist, H., D. Maring, T. Thurn-Albrecht, and U. Wiesner, "Double flip of orientation for a lamellar diblock copolymer under shear," J. Chem. Phys. **110**, 8225 (1999).

Leslie, F. M., "Some constitutive equations for anisotropic fluids," Q. J. Mech. Appl. Math. **19**, 357 (1966).

Maring, D., and U. Wiesner, "Threshold strain value for perpendicular orientation in dynamically sheared diblock copolymers," Macromolecules **30**, 660 (1997).

Martin, P. C., O. Parodi, and P. S. Pershan, "Unified hydrodynamic theory for crystals, liquid crystals, and normal fluids," Phys. Rev. A **6**, 2401 (1972).

Matsen, M. W., "Kink grain boundaries in a block copolymer lamellar phase," J. Chem. Phys. **107**, 8110 (1997).

Maurits, N. M., A. V. Zvelindovsky, G. J. A. Sevink, B. A. C. van Vlimmeren, and J. G. E. M. Fraaije, "Hydrodynamic effects in three-dimensional microphase separation of block copolymers: Dynamic mean-field density functional approach," J. Chem. Phys. **108**, 9150 (1998).

Netz, R. R., D. Andelman, and M. Schick, "Interfaces of modulated phases," Phys. Rev. Lett. **79**, 1058 (1997).

Ohta, T., Y. Enomoto, J. L. Harden, and M. Doi, "Anomalous rheological behavior of ordered phases of block copolymers. 1," Macromolecules **26**, 4928 (1993).

Ohta, T., and K. Kawasaki, "Equilibrium morphology of block copolymer melts," Macromolecules **19**, 2621 (1986).

Patel, S. S., R. G. Larson, K. I. Winey, and H. Watanabe, "Shear orientation and rheology of a lamellar polystyrene-polyisoprene block copolymer," Macromolecules **28**, 4313 (1995).

Pinheiro, B. S., D. A. Hajduk, S. M. Gruner, and K. I. Winey, "Shear-stabilized bi-axial texture and lamellar contraction in both diblock copolymer and diblock copolymer/homopolymer blends," Macromolecules **29**, 1482 (1996).

Pinheiro, B. S., and K. I. Winey, "Mixed parallel-perpendicular morphologies in diblock copolymer systems

correlated to the linear viscoelastic properties of the parallel and perpendicular morphologies," Macromolecules **31**, 4447 (1998).

Qiao, L., and K. I. Winey, "Evoluton of kink bands and tilt boundaries in block copolymers at large shear strains," Macromolecules **33**, 851 (2000).

Soddemann, T., G. K. Auernhammer, H. Guo, B. Dünweg, and K. Kremer, "Shear-induced undulation of smectic-A: Molecular dynamics simulations vs. analytical theory," Eur. Phys. J. E **13**, 141 (2004).

Wang, Z.-G., "Response and instabilities of the lamellar phase of diblock copolymers under uniaxial stress," J. Chem. Phys. **100**, 2298 (1994).

Williams, D. R. M., and F. C. MacKintosh, "Shear of diblock copolymer lamellae: Width changes and undulational instabilities," Macromolecules **27**, 7677 (1994).

Wu, L., T. P. Lodge, and F. S. Bates, "Bridge to loop transition in a shear aligned lamellae forming heptablock copolymer," Macromolecules **37**, 8184 (2004).

Wu, L., T. P. Lodge, and F. S. Bates, "Effect of block number on multiblock copolymer lamellae alignment under oscillatory shear," J. Rheol. **49**, 1231 (2005).

Xu, A., G. Gonnella, A. Lamura, G. Amati, and F. Massaioli, "Scaling and hydrodynamic effects in lamellar ordering," Europhys. Lett. **71**, 651 (2005).

Yih, C. S., "Instability due to viscosity stratification," J. Fluid Mech. **27**, 337 (1967).

Yih, C. S., "Instability of unsteady flows or configurations: Part 1. Instability of a horizontal liquid layer on an oscillating plane," J. Fluid Mech. **31**, 737 (1968).